Nuclear Technology

ISSN: 0029-5450 (Print) 1943-7471 (Online) Journal homepage: https://www.tandfonline.com/loi/unct20

A Note on the Use of Uranine Tracer to Visualize Radionuclide Migration Experiments: Some Observations and Problems

Helen Winberg-Wang, Ivars Neretnieks & Mikko Voutilainen

To cite this article: Helen Winberg-Wang, Ivars Neretnieks & Mikko Voutilainen (2019): A Note on the Use of Uranine Tracer to Visualize Radionuclide Migration Experiments: Some Observations and Problems, Nuclear Technology, DOI: 10.1080/00295450.2019.1573620

To link to this article: https://doi.org/10.1080/00295450.2019.1573620

Published online: 25 Mar 2019.

NUCLEAR TECHNOLOGY

DOI: https://doi.org/10.1080/00295450.2019.1573620

A Note on the Use of Uranine Tracer to Visualize Radionuclide Migration Experiments: Some Observations and Problems

Helen Winberg-Wang,[a]* Ivars Neretnieks,[a] and Mikko Voutilainen[b]

[a]*Royal Institute of Technology, Department of Chemical Engineering, Stockholm, Sweden*
[b]*University of Helsinki, Department of Chemistry, Helsinki, Finland*

Received December 3, 2018
Accepted for Publication January 19, 2019

Abstract — *Uranine is a dye commonly used in tracer experiments; it is chosen for its high visibility even at low concentrations. Uranine solutions are slightly denser than water at the same temperature. However, in laboratory experiments uranine solutions have been known to occasionally show unpredictable flow behaviors. This paper investigates the possible effect of light-induced density change to explain some of these behaviors. Uranine has a wide light absorption spectrum for visible light, which can heat the dye solution and lower its density to below that of the surrounding water, which induces buoyancy-driven flow. Simulations are made in both one dimension and two dimensions to determine the extent of the effect. The results are then compared to different experiments with unanticipated flow patterns.*

Keywords — *Uranine/fluorescein tracer experiments, flow patterns in fractures, light-induced density-driven flow, buoyancy flow in fractures.*

Note — *Some figures may be in color only in the electronic version.*

I. INTRODUCTION AND BACKGROUND

It is well known that differences in local temperature and solute concentration in water can cause buoyancy-induced flow in bodies of water. There is a vast amount of literature on the subject, e.g., publications by Elder,[1] Voss and Souza,[2] Holzbecher,[3] Moukalled et al.,[4] and López and Smith,[5] to name only a few. Moukalled et al.[4] cite a large number of papers that describe buoyancy processes in narrow annuli of various types and how flow patterns can be simulated by numerical methods.

Buoyancy-induced flow can also take place in narrow fractures in fractured crystalline rocks such as bedrock used to host repositories for radioactive waste. Buoyancy effects due to temperature differences generated by the heat emanating from the decay of radionuclides and intrusion of salt or meteoric water are accounted for when modeling flow pattern evolution over time and space in the Swedish and Finnish KBS-3 types of designs for high-level nuclear waste repositories in fractured crystalline rocks.[6,7a] Also, the exchange of dissolved salt by molecular diffusion in and out of the slightly porous rock matrix to and from the mobile water in the fractures is accounted for in the models.[8] Recently, it has also been shown that salt exchange between the bentonite clay used to enclose the waste canisters in deposition holes and waste in vault repositories can generate local convection currents that can increase the release rate of nuclides.[9] These narrow but rapid currents can move long distances before they are diluted by mixing with other waters.

There is a desire by authorities that license the construction of radioactive waste repositories to demonstrate that the various design components and the underlying

*E-mail: helenwi@kth.se

[a] Reports can be downloaded at http://www.Posiva.fi/reports and http://www.skb.se/publication.

theories and models used in the safety analyses are valid and robust. This also applies to modeling of the mass transfer processes that govern radionuclide release from repository components to the seeping water in the fractures. This mass transfer constitutes one of the important transfer resistances to radionuclide release.

We set out to visualize experimentally the mass transfer rate in narrow-constant-aperture and variable-aperture slots simulating a fracture in crystalline rock in which seeping water passes and contacts a source of tracer that diffuses out into the water as it seeps by. The flow velocities were chosen to be in the range expected under natural conditions, i.e., 1 m/yr up to hundreds of meters per year. The residence time in the fracture replica was chosen to be on the order of 1 month in order to give the tracer time to diffuse about 10 cm before being swept away. This would cover a few correlation lengths in the variable-aperture fracture and would be sufficient to be within a realistic range of aperture variations.

We primarily used uranine (fluorescein) as tracer because it can be detected in very low concentrations. During this work, it was found that even weak illumination in the laboratory heats up the tracer solution and gives rise to circulation patterns that would not be present without light absorption. Also, blackbody radiation to and from the walls was suspected to induce circulation. This prevented the direct visualization and validation of the mass transfer to seeping water. Instead, an indirect method was devised that visualized and demonstrated the diffusive transport to seeping water.[10]

Recently, a flow pattern of another experiment, designed to study an effect of matrix diffusion on transport radioactive tracer pulse flowing in a narrow annulus between a concentric tube and a centered drill core,[11] was visualized using uranine. The outer tube was transparent to be able to observe the flow pattern. A short pulse of the uranine tracer was injected into an upward water flow in the annulus. The equipment was manufactured with great care to ensure that the annulus had a minimal variation in the aperture. The water distribution device at the bottom of the slot was specifically designed to ensure that the inflow was evenly distributed in the annulus. The flow rate was very low, chosen to be comparable to that of a long-term field experiment with a similar annulus size.[12] The water residence times in two experiments with 1- and 2-mm apertures were several hundred hours in the laboratory experiments. The upward propagation of the uranine pulse was followed by photographs and movies. In the initial stage, a plug flow was seen, but after a short time, i.e., hour(s), prominent "fingering" developed and rose rapidly. These results suggested extremely large dispersion effects. This was initially interpreted as maldistribution of the forced flow due to aperture variations. Alternatively, such an effect could be caused by light-induced heating of the laboratory lighting. Furthermore, similar experiments performed in gas phase using helium as tracer and a nontransparent tube did not show the effect by channeled flow field,[13] which supports the light-induced-effect explanation.

In the present paper, we explore how absorption of light in the traced solution can induce flow and/or give rise to abnormal flow rate distribution in narrow slots. To the best of our knowledge, light-induced buoyancy has not been described earlier in the context of investigations related to radioactive waste repository design. Our results could influence the design of future tracer experiments in transparent variable-aperture fractures, in which hydraulically induced low-velocity flow patterns and solute transport are studied.

II. AIMS AND SCOPE

We wish to explore how light absorption of a dye, i.e., uranine, in a transparent vertical slot can generate buoyancy flow that disturbs and overpowers the flow pattern induced by hydraulic gradients. Such disturbance can generate fluid circulation and cause hydrodynamic dispersion that would not develop otherwise. Insights into the processes can aid in designing necessary visualization experiments that are not subject to this disturbing effect.

III. AN EXPERIMENT THAT SHOWS BUOYANCY-INDUCED FLOW IN A NARROW SLOT

Uranine, an organic fluorescing dye, has been widely and successfully used in field tracer experiments because it can be visually detected even in very low concentrations. Below, we describe a simple experiment in which low light intensity rapidly induced flow. This experiment will be modeled later.

An experimental device was constructed by separating two (25 × 25-cm) acrylic glass sheets with 1-mm spacers. The sides were then sealed with silicon. The device, called a slot, was mounted vertically with one corner lowest, with a 45-deg angle to the table, as seen in Fig. 1. The slot was placed in front of a light board. The slot was filled with water through tubes attached to the side corners. For the injection of the dye, a silicon plug was located in the lower corner, and a fine syringe needle was inserted in the top corner to remove air and to even out the internal pressure during the dye injection.

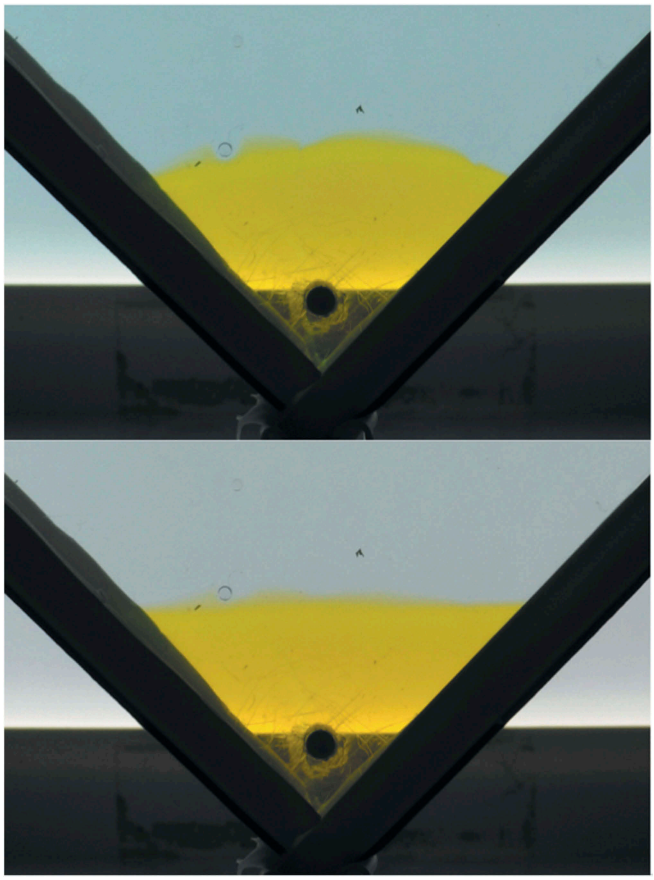

Fig. 1. Top frame: The dye blob in the slot right after injection through the plug. Bottom frame: The same blob 50 s after injection.

In the experiment, the slot was first filled with degassed deionized water and left to rest to avoid initial convection. A small volume of uranine solution, 0.5 mL of 1.75 g/L, was slowly injected with the syringe, through the silicon plug, which acted like a self-sealing membrane. Initially, the uranine blob was slightly convex around the injection location. After less than 1 min, it flattened and settled in the bottom corner; see Fig. 1.

The temperature in the laboratory was around 20°C, and the light intensity of the light screen behind the slot is around 2000 lm/m^2 with daylight color temperature. The entity lm (lumen) is the SI unit of luminous flux. Points on the slot receive around 1500 lm/m^2 as some of the light passes outside the slot. The light board was the main source of illumination in the laboratory and the only illumination when the laboratory was not in use.

Figure 2 shows how the "heavy" uranine blob "wobbles" slowly during the first hour and suddenly emits a narrow stream at 1 h and 23 min. Figure 2 also shows how the narrow stream rapidly rises in the slot. The entire blob becomes unstable and after 9 h and 47 min has disintegrated and the dye has risen to the top of the slot. The photographs in Fig. 2 show different times of the uranine blob's injection into the bottom corner and its fate. In the photographs, to enhance visibility, Photoshop® (Ref. 14) was used to transform the original yellow-green color of uranine to blue.

By enlarging the lower part of the slot in the last frame in Fig. 2, as can be seen in Fig. 3, well-defined Rayleigh-Taylor fingers can be observed. Rayleigh-Taylor fingers appear when a liquid of lower density presses up through a liquid of higher density.[15] This shows that the dye has changed from a liquid with a density higher than water (Fig. 1) to a liquid with a density lower than water.

IV. BUOYANCY AND RAYLEIGH INSTABILITY

When a less-dense fluid underlies a denser fluid, the system is inherently unstable. Holzbecher[3] discusses how such instabilities can be modeled in the context of flow in radionuclide waste repositories in porous and fractured rock. He presents models and computation tools to describe the flow patterns generated. He also discusses the Rayleigh-Taylor instability in that context.

The competing processes that generate the driving force, i.e., the buoyancy due to density differences and the restraining force (that is, the friction of the mobilized fluid as it moves in the narrow slot), change over time. Initially, the density difference between a spot with dye (heavy liquid) and surrounding pure water (light liquid) is positive, and the dyed spot will tend to sink or stay at the bottom. As the dyed liquid is heated by absorbing light energy, it will become less dense. The dyed spot, when it becomes lighter than the pure water, will rise. When the driving force and thus the velocity are small, heat conduction between the spot and the surrounding water and walls of the slot will have time to cool the spot and decrease the velocity and stabilize the flow. When the driving force is large, the spot may not be cooled as rapidly as it is heated by absorption of more light, and therefore, it can accelerate. This leads to instability and can cause circulation patterns. The situation is further complicated by molecular diffusion of the dye molecules from the spot to the pure water. The spot is diluted and grows. If the dye concentration initially is very high so that "all" light is absorbed, a growing spot, although diluted, will still be able to absorb practically all light and maintain its driving force per the volume of the spot. The driving force will decrease if the dilution leads to less light absorption per volume of the spot. Thus, we have to account for a number of processes that influence the

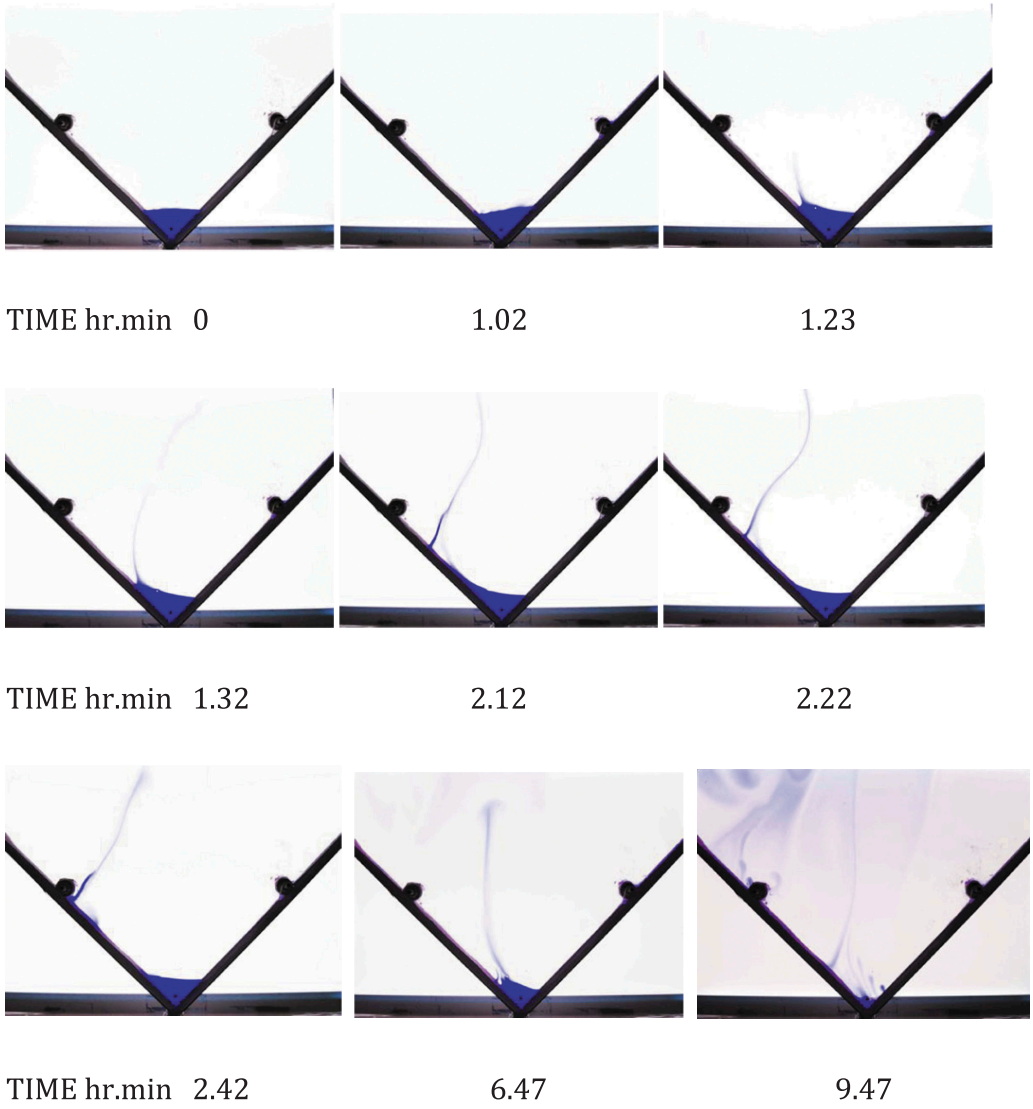

Fig. 2. Development of rising flares of uranine. Original light yellow-green color has been transformed to blue using Photoshop.

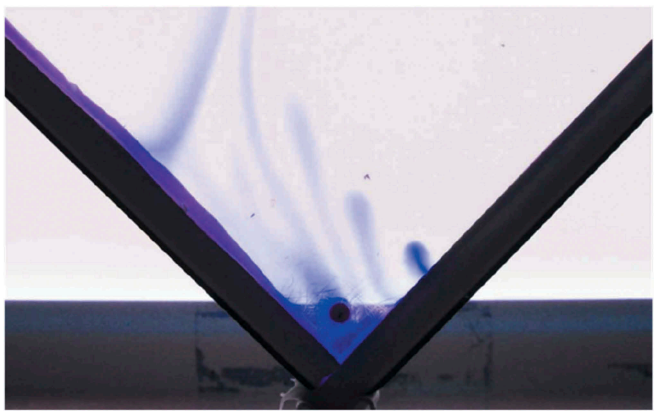

Fig. 3. Enlargement of the bottom portion of the last frame in Fig. 2.

buoyancy and stability of the system when modeling the evolution of flow in the slot.

V. MATHEMATICAL MODEL

V.A. Model

The coupled processes outlined in Sec. IV are formulated in a mathematical model in this section.

To account for local density gradients due to the diffusion-propagation and the density-driven flow, the system is described in two dimensions. The horizontal and vertical directions are denoted x and z, respectively.

The temperature and fluid density in the third direction, i.e., over the thickness of the slot, are assumed to be constant. This is supported by scoping calculations. The following set of equations that govern the diffusion, flow, and heat transport in the slot and the immediate surroundings is used to simulate the buoyancy-induced flow in the slot.

The flow field, as a function of density $\rho(T,c)$, is described by the continuity equation [Eq. (1)] in combination with the Darcy equation [Eqs. (2) and (3)]:

$$\frac{\partial \rho(T,c)}{\partial t} + \frac{\partial \rho(T,c)u_x}{\partial x} + \frac{\partial \rho(T,c)u_z}{\partial z} = 0 \ , \tag{1}$$

$$u_x = -\frac{\kappa}{\mu(T)}\frac{\partial p}{\partial x} \ , \tag{2}$$

and

$$u_z = -\frac{\kappa}{\mu(T)}\left(\frac{\partial p}{\partial z} + \rho(T,c)g\right) \ , \tag{3}$$

where

$u_x,\ u_z$ = velocities in the x-direction and z-direction, respectively

$\kappa = \frac{\delta_{fr}^2}{12}$ = permeability

$\mu(T)$ = water viscosity.

Initially, there is no flow present in the slot, with the aperture δ_{fr}, and the pressure in the slot is described by $p = \rho g h$.

The mass transport is described by the diffusion-convection equation:

$$\frac{\partial \overline{c}}{\partial t} = -u_x\frac{\partial \overline{c}}{\partial x} - u_z\frac{\partial \overline{c}}{\partial z} + D_w\left(\frac{\partial^2 \overline{c}}{\partial x^2} + \frac{\partial^2 \overline{c}}{\partial z^2}\right) \ , \tag{4}$$

where D_w is the diffusivity of uranine; $\overline{c}$ and $\overline{c}_O = 1$ are the normalized concentration and the initial normalized concentration, when the former is defined from the initial concentration c_O as

$$\overline{c} = \overline{c}_O\frac{c}{c_O} \ . \tag{5}$$

The temperature evolution in the system is treated as three two-dimensional (2-D) domains: one for water and two for acrylic glass, with aperture δ_p; one acrylic glass sheet is on each side of the water slot. The temperature in the water domain is described by the equation of energy in combination with Fourier's law of heat conduction:

$$\begin{aligned}&\rho(T,c)C_{p,w}\frac{\partial T}{\partial t} + \rho(T)C_{p,w}\left(u_x\frac{\partial T}{\partial x} + u_z\frac{\partial T}{\partial z}\right)\\ &- k_w\left(\frac{\partial^2 T}{\partial x^2} + \frac{\partial^2 T}{\partial z^2}\right) = Q - \frac{q_{a(front)} + q_{a(back)}}{\delta_{fr}} \ ,\end{aligned} \tag{6}$$

where Q is the energy flux caused by absorbed light. The heat emanating from the absorbed light is described by the Lambert-Beers law [Eq. (7)]:

$$Q = \frac{q_o}{\delta_{fr}}\left(1 - 10^{-\varepsilon c \delta_{fr}}\right) , \tag{7}$$

where

c = molar concentration

q_o = power flux

δ_{fr} = slot aperture

ε = mean absorption coefficient.

The value q_a is the heat flux from the water to the acrylic glass on each side, which is given by

$$q_{a(side)} = k_a \cdot \frac{\left(T_w - T_{a(side)}\right)}{\delta_a} \ . \tag{8}$$

The two sides can have two different surface temperatures $T_{a(side)}$. The acrylic glass temperatures are simultaneously simulated with heat coming from the water, $q_{a(side)}$, inside the slot and heat leaving the surroundings, $q_{fc(side)}$, via natural convection and blackbody radiation to the outer sides of the acrylic glass:

$$\rho C_{p,a}\frac{\partial T}{\partial t} - k_a\left(\frac{\partial^2 T}{\partial x^2} + \frac{\partial^2 T}{\partial z^2}\right) = \frac{q_{a(side)} - q_{fc(side)}}{\delta_a} \tag{9}$$

and

$$q_{fc(side)} = h_a \cdot (T_o - T) + \sigma_{BB}\, e_{Gray}\left(T_{surr(side)}^4 - T_{a(side)}^4\right) , \tag{10}$$

where

T_o = ambient temperature

T_{surr} = surrounding (wall, ceiling, and light board) temperature

$h_a,\ \sigma_{BB}\, e_{Gray}$ = heat transfer coefficients by convection and blackbody radiation to air

and surrounding walls

h_a = function of H and ΔT, which are described in detail in Sec. V.B.

V.A.1. Initial and Boundary Conditions

For the simulation of the experiment shown in Fig. 2, the mass transport is described by the diffusion-convection equation for a sealed slot. The two velocity components are zero initially, and the initial concentration for the triangle filled with dye is described by

$$\overline{c}(t=0) = \begin{cases} 0 & z > 0.022 \text{ m} \\ \overline{c}_O & z = < 0.022 \text{ m} \end{cases} . \tag{11}$$

Initially, the whole setup is at ambient temperature, and the sides are assumed fully insulated, with no mass or heat flux in the x-direction and z-direction beyond the slot.

V.B. Data Section

The density function for the slot is described as the sum of the temperature-dependent water density plus the initial mass concentration of dye times the normalized local concentration by the following equation of state used for low concentrations:

$$\rho(T) = \rho_T \left(1 - \frac{c_O \cdot \frac{\overline{c}}{\overline{c}_O}}{\rho_U} \right) + c_O \cdot \frac{\overline{c}}{\overline{c}_O} , \tag{12}$$

where

ρ_U = 1600 kg/m^3 (Ref. 16)

ρ_T = function that expresses the water density as a function of temperature, presented by Jones and Harris[17]

c_O = initial dye concentration of uranine in the solution (kg/m^3).

The partial volume of uranine in the solution is approximated from the density of the uranine crystals.

Sjöback et al.[18] measured absorption spectra of uranine solutions in water at different pH, salinities, and concentrations. In neutral and slightly basic solution, the di-ionic form dominates. The peak extinction coefficient at 490 nm is 76 900 $M^{-1}\cdot\text{cm}^{-1}$. In the wavelength range of 400 to 550 nm, it has a mean extinction coefficient of ϵ = 13 500 $M^{-1}\cdot\text{cm}^{-1}$ (Ref. 18). This was confirmed by light absorption measurements of the dye solution.

A Microlight Tokar #6833-A4 light screen with a cold cathode fluorescent lamp (CCFL) tube gives 2000 lm/m^2 as measured by the light meter used (Standard ST 1300, Clas Ohlson). At the location of the slot, 5 cm distant, it is 1500 lm/m^2. It is related to the energy in the light photons times the sensitivity of the human eye at a given wavelength integrated over the wavelengths at which the eye is sensitive, i.e., 400 to 700 nm. The absorbed light energy in the uranine heats the water. To convert the lumens per meters squared to watts per meters squared, the spectral distribution of the light source is needed. This can be calculated using the luminous efficacy η_s (lumens per watt).

The luminous efficacy of a blackbody radiator (the sun) at 5800 K in the range of visible light 400 to 700 nm (ideal "white" source) is 251 lm/W (Ref. 19). However, the light from the light screen is generated by the fluorescent source, which emits the energy in a few narrow spectral lines that together with the human eye is perceived as white light. Murphy[19] in an example cites a value as high as 349.1 lm/W when integrating over the spectral lines in the visible range. However, there are also a few spectral lines with high intensity in the range 400 and 430 nm, where the human eye has a rather low photopic sensitivity and thus contributes with only a few lumens per watt. In the literature, CCFL tubes are stated to have a luminous efficacy in the range of 26 to 60 lm/W (Refs. 20, 21, and 22), and the average is what will be used as an estimate in the following examples. A luminous efficacy of 43 lm/W together with the measurement of the light screen gives a power flux of about 35 W/m^2 at the slot. Part of this light energy can then be absorbed by the dye to heat the fluid, equipment, and air.

V.B.1. Heat Transfer Coefficients for Convective and Radiation Cooling of Slot

For free convection at a vertical surface, the heat transfer coefficient can be estimated from the following expressions[23]:

$$h_{conv} = \frac{k_{air}}{H} 0.518 \ (Gr_T \text{Pr})^{0.25} \tag{13}$$

and

$$Gr_T = \frac{\rho_{air}{}^2 g \ \beta_T \Delta T H^3}{\eta_{air}{}^2} , \tag{14}$$

where

β_T = thermal expansion coefficient:

$$\beta_T = \frac{1}{\rho_{air}} \frac{d\rho_{air}}{dT} = -\frac{1}{T} \cong -3.5 \times 10^{-3} (1/\mathrm{K}) \qquad (15)$$

ΔT = temperature difference between air and surface

H = height of the surface area that is heated

ρ_{air} = air density; μ_{air} is its viscosity

Pr = Prandtl number = 0.7 for air.

For air at ambient temperature, the convective heat transfer coefficient is

$$h_{conv} = 1.25\ H^{-1/4}\ \Delta T^{1/4} \qquad (16)$$

in units of watts per meters squared times degrees kelvin using the entity of H in units of meter.

These relations are valid when the entire surface has a constant temperature that deviates by ΔT from the surrounding air. It is not strictly valid for the problem at hand because ΔT changes with time as the slot is heated by the radiation from the light screen that is absorbed by the uranine. Furthermore, the uranine concentration is not evenly distributed in the slot. It would be valid when the uranine has been equally distributed in the slot by diffusion and by the induced convection currents. The convective heat transfer is used to illustrate that natural convection will be active and that it will cool the slot to some degree.

In contrast, blackbody radiation acts directly on each location in the slot. The temperature in the acrylic glass quite rapidly adapts to the temperature in the water in each location in the slot. It is only damped in time by the time a heated spot distributes its heat locally into the acrylic glass. The characteristic time for thermal adjustment, $\frac{1}{t_c} = \frac{dx^2}{D_{th}}$, is a few minutes for acrylic glass 4 mm thick; D_{th}, as a function of $\frac{k}{\rho c_p}$, is given in Table I.

The heated locations in the slot also emit energy by blackbody radiation and receive radiation from the surroundings with net flux equal to (the flux is over the spherical angle that has temperature T_1 in one point on the slot and T_2 at the surroundings)

$$q_{light} = \sigma_{BB}\ e_{Gray} (T_1^4 - T_2^4)\ , \qquad (17)$$

where e_{Gray} is the emissivity of the surfaces, in this case, assumed to be the same for the heated spot and the cooler walls of the room, which together with the slightly warmer light board entirely surrounds the equipment. σ_{BB} is the Stefan-Boltzmann constant for blackbody radiation; its value is $5.67 \times 10^{-8}\ \mathrm{W/m^2 \cdot K^{-4}}$.

The value e_{Gray} is an empirical factor, less than 1, that accounts for deviation from blackbody radiation. For polished shiny metal surfaces, e_{Gray} can be much less than zero. For most materials, it is slightly below 1 (Ref. 23). We take it to be 0.9 for both the heated spot and the surroundings.

Blackbody radiation from the light screen, which is marginally warmer than the surroundings, can also be accounted for. The screen is located at a short distance from the slot and covers a considerable fraction of the horizon on that side. This can in principle be determined by integrating the radiation to and from the heated spot over the entire spherical direction using Bird et al.'s view factor concept.[23] This is not practical because the temperature of the light screen has variations of 0.5 K. This is in the same range as the steady-state heating of the spots, in which there is uranine that is heated by the screen radiation by visible light. Also, the surrounding walls vary in temperature by a fraction of 1 K and local heat sources from laboratory equipment. However, undetermined external heat sources are more likely to have a greater effect on the water temperature than the dye temperature due to its larger ΔT.

The maximum cooling by blackbody radiation will be when the light screen has the same temperature as the

TABLE I

Material Properties for the Media*

	ρ (at 20°C) (kg/m^3)	c_p (kJ/kg·K^{-1})	k_{th} (at 25°C) (W/m·K^{-1})	η_a (Pa s)	D_{th} (m^2/s)
Water		4.18	0.60	10^{-3}	1.4×10^{-7}
Acrylic glass	1190	1.5	0.2	–	1.1×10^{-7}
Air	1.20	1.0	0.026	1.8×10^{-5}	–

*Material properties for the media are from Refs. 24 through 29. The diffusivity of uranine in water is 6.4×10^{-10} m^2/s (Ref. 30).

other surroundings. Then, ΔT is constant over the entire surroundings. When the screen has a temperature slightly higher than the surroundings, Eq. (17) can be used to determine the contribution from this by integrating over the spherical angle region covered by the screen.

The problem is further complicated when a person or persons are present in the laboratory during the experiments and are close to the equipment. Physical contact with, as well as blackbody radiation from, a warm body can heat the equipment. We will explore how these uncertainties influence the buoyancy by simple sensitivity simulations.

Given the maximum blackbody radiation loss for a small difference ΔT, the flux at room temperature (293 K) can then be described by linearizing Eq. (17) around T_1 or T_2. This gives

$$q_{light} = h_{rad}\Delta T = \ 5.13\ \Delta T\ . \tag{18}$$

The contribution from convection and maximum blackbody radiation gives a heat transfer coefficient

$$q_p = 1.25\ H^{-1/4}\ \Delta T^{5/4} + \ 5.13\ \Delta T\ . \tag{19}$$

VI. RESULTS

VI.A. Some Illustrative Calculations

Figure 4 shows the fraction of light absorbed as a function of the uranine concentration in a 1-mm-aperture slot. Concentrations as low as 0.01 g/L uranine will absorb 9% of the light, and even 0.001 g/L will absorb 0.93% of the visible light.

Below, we explore how noticeable heating and buoyancy can be caused by light absorption in the tracer. Referring to the experiments described above, consider a tracer blob, with a slightly larger density than water, injected in the bottom of a slot. The blob begins to heat up, and its density decreases. When its density becomes less than that of the surrounding water, it can start to rise.

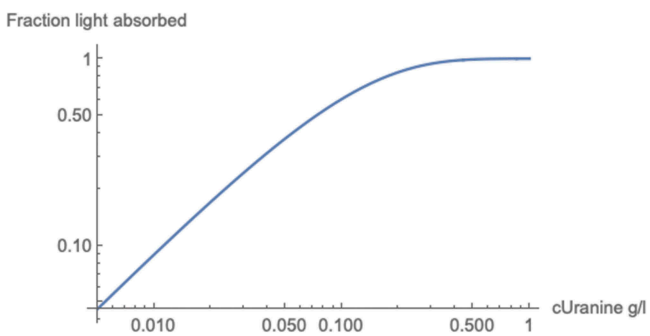

Fig. 4. The fraction of light absorbed in a 1-mm-aperture slot as a function of the uranine concentration.

VI.B. Temperature Rise in the Slot

To gain an impression of how the water in the slot would increase its temperature if there was no heat loss to the surroundings, we exemplify this for the 1-mm-aperture slot into which all the absorbed energy of the light is deposited. The temperature rise rate for $q_o = 35\ \mathrm{W/m^2}$ is $\frac{dT}{dt} = \frac{q_o}{\delta_w \rho_w c_{p,w}} = 30.1$ K/h. If one accounts also for the heat capacity of the acrylic glass that is heated, the temperature rise would be reduced to 6.7 K/h.

Further, accounting for the heat loss to the surroundings by convection and radiation, the steady-state temperature of the slot can be obtained from the energy balance:

$$\begin{aligned} q_{light} &= q_o(1 - 10^{-\epsilon c \delta_{wcm}}) = q_{loss,tot} \\ &= 2 \times \left(1.25\ H^{-1/4}\Delta T^{5/4} + 5.13\right) \\ &\quad \times \Delta T\ (\text{loss on two sides})\ . \end{aligned} \tag{20}$$

Figure 5 shows the steady-state temperature rise in a 1-mm slot filled with uranine solutions of different concentrations and a free-convection height H of 0.25 m.

Initially, the tracer solution is denser than the water above but gradually becomes less dense as it heats up. If there are no convection currents and no thermal conduction in the x-direction and z-direction,

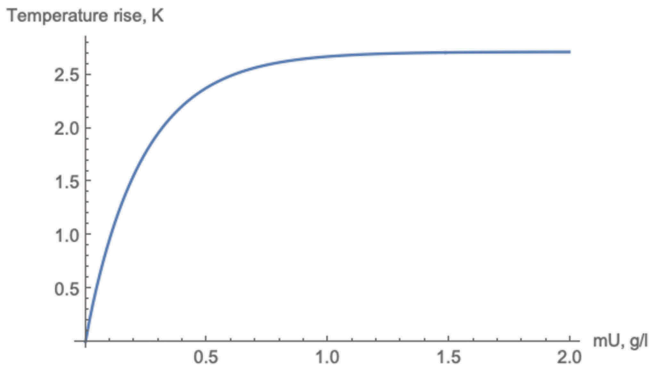

Fig. 5. Steady-state temperature rise in a 1-mm slot filled with uranine solutions of different concentrations. The heat capacity of water and acrylic glass are accounted for; $q_o = 35\ \mathrm{W/m^2}$.

the density evolution of the dye solution can be determined by

$$\left(\rho_w c C_{pw}\delta_w + 2\rho_a C_{pa}\delta_a\right)\frac{\partial \Delta T}{\partial t} = q_o 10^{-\epsilon c \delta_{w,cm}} - 2\left(1.25\, H^{-\frac{1}{4}}\,\Delta T^{\frac{1}{4}} + 5.13\Delta T\right), \quad (21)$$

where

ρ = density

C_p = heat capacity

δ = thickness

w, a = indices that stand for water and acrylic glass, respectively.

Scoping calculations show that the heat spreads so quickly, i.e., in minutes, in the acrylic glass that in practice it is in thermal equilibrium with the water, which implies that Eq. (21) is a good approximation of the time evolution of the temperature rise.

Figure 6 shows the temperature increase above ambient in a 1-mm-aperture slot for different concentrations of uranine for q_o = 35 W/m^2 and 15 W/m^2, respectively. Higher uranine concentrations do not cause larger temperature increases because already 1 g/L absorbs practically all visible light energy.

The density of the solution is initially larger than that of pure water at the same temperature. A spot with uranine is therefore "heavier" than the surrounding water without dye. However, when the spot with water absorbs light, which heats it, it gradually becomes lighter than the water without dye, which is not heated by light absorption. If the spot becomes lighter than the surrounding water, it will start to rise.

For q_o = 35 W/m^2, as can be seen in Fig. 7a, the density difference decreases from positive to negative after 1 h for all uranine concentrations in the slot. For q_o = 15 W/m^2, as can be seen in Fig. 7b, it remains positive only for concentrations above 0.8 g/L.

VI.C. Simulations of Development of Flow Currents in the Slot

The 2-D simulations were made using COMSOL Multiphysics[31] and its Material Library (water and acrylic plastic) for the system shown in Fig. 2. The slot is 25 × 25 cm and has a 1-mm aperture, surrounded by two sheets of acrylic glass with a thickness of 4 mm. Radiation and free convection act on both outer surfaces. The natural convection heat transfer coefficient is estimated by COMSOL with the standing height of the tilted slot and a room temperature of 20°C. However, the complexity of the domain, such as temperature gradients in both the x-direction and z-direction and its irregular height, in z, makes it difficult to account for the free convection fairly.

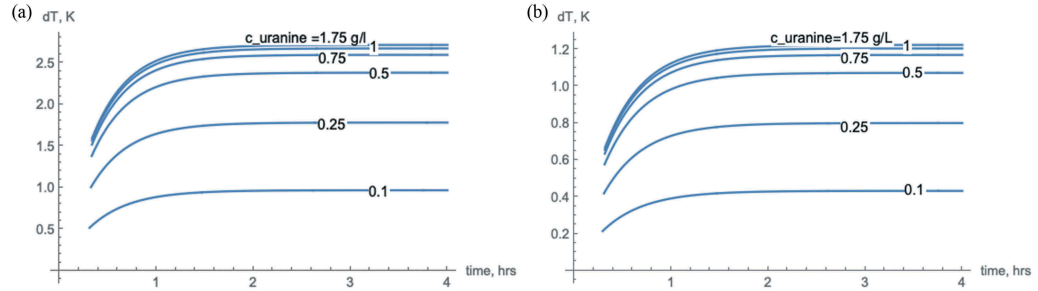

Fig. 6. Temperature increase above ambient for different concentrations of uranine for (a) q_o = 35 W/m^2 and (b) q_o = 15 W/m^2.

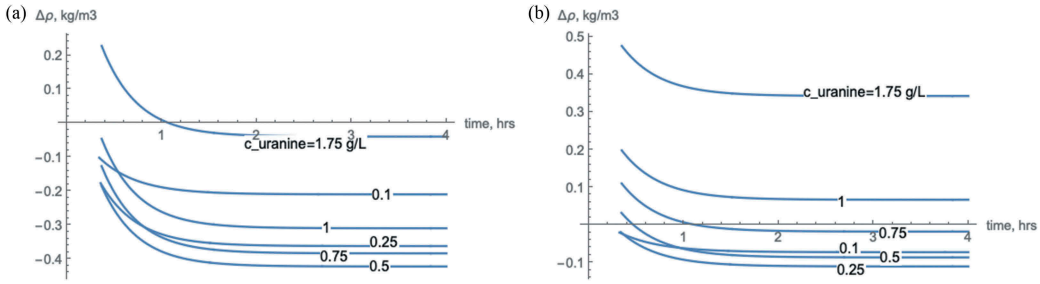

Fig. 7. Density difference decrease for different concentrations of uranine for (a) q_o = 35 W/m^2 and (b) q_o = 15 W/m^2.

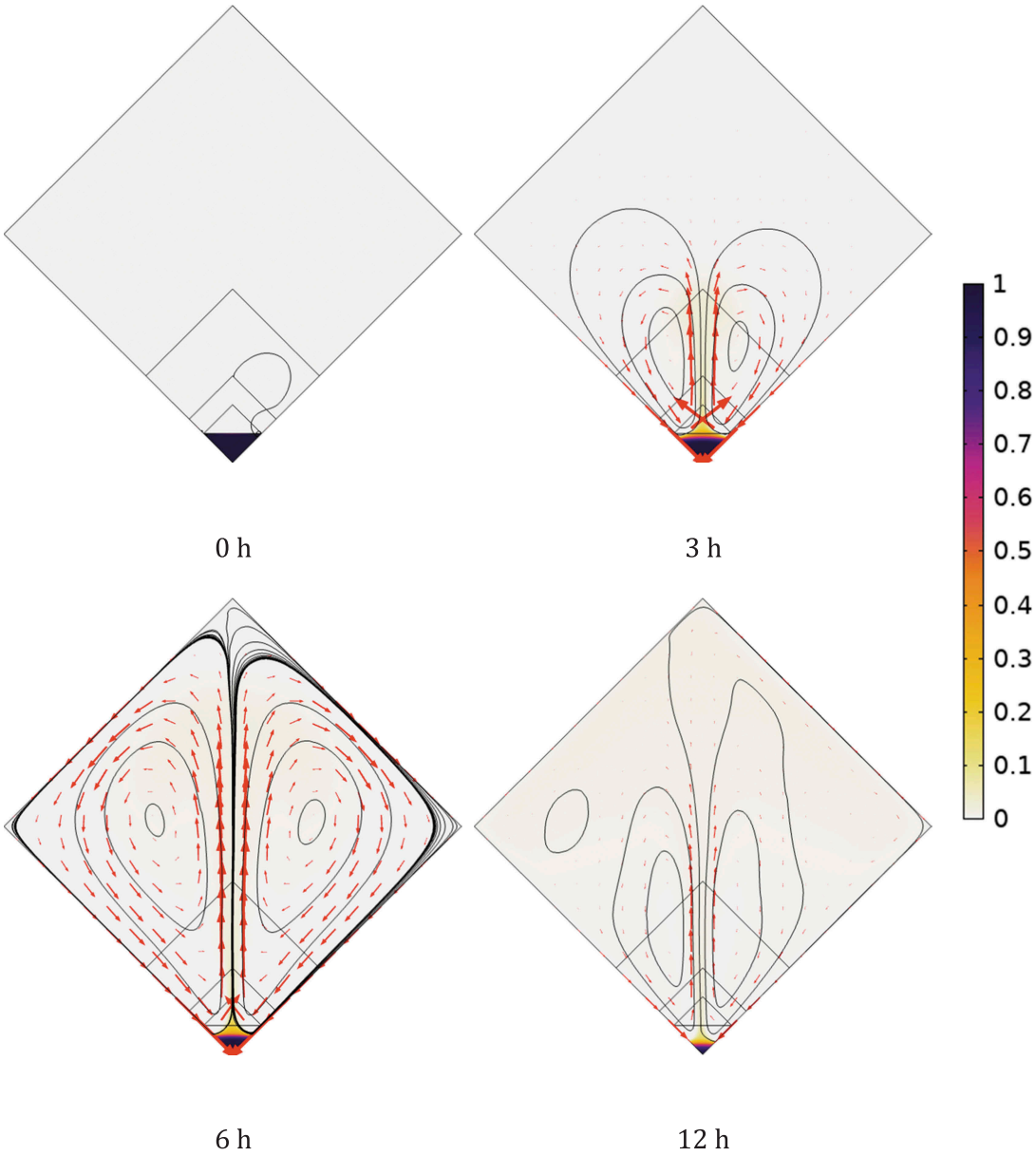

Fig. 8. Diffusion, convection, and heat simulation for the tilted slot. The solid curved lines and the arrows describe the streamlines and the flow field, respectively. The color bar indicates the normalized concentration of uranine dye.

To account for blackbody radiation, room temperature is used on the room side, and 2°C warmer on the light board side is used to account for the slightly warmer surface. The uranine concentration was initially 1.75 g/L below $y = 22$ mm and zero in the remainder of the domain. The results are presented in Fig. 8 for four different instances in time.

For a light exposure of 35 W/m^2, as can be seen in Fig. 8, the onset of circulation is after less than 1 h, and the uranine has essentially been diluted in the entire water volume in the slot after 12 h. This is in overall agreement with what was observed in the experiments.

Rayleigh-Taylor fingering with very narrow streams has not been simulated by the model because it would need excessively finer discretization and a more detailed modeling of the heat transfer from the water into and within the acrylic glass. The simulated general flow pattern supports the observations that convection currents will develop. The asymmetric and wobbling flow pattern, shown in Fig. 2, suggests the onset of Rayleigh-Taylor instability. A simulation with q_o = 1 W/m^2 did not result in circulation patterns but showed a stable heat gradient with a slightly higher temperature in the region with dye. In

simulations with larger q_o, circulation started earlier as did simulations with lower convective and radiation heat transfer coefficients.

The uranine transport experiments in the annular flow channel designed by Voutilainen et al.[11] were investigated by applying the above simulation procedure, with one of the

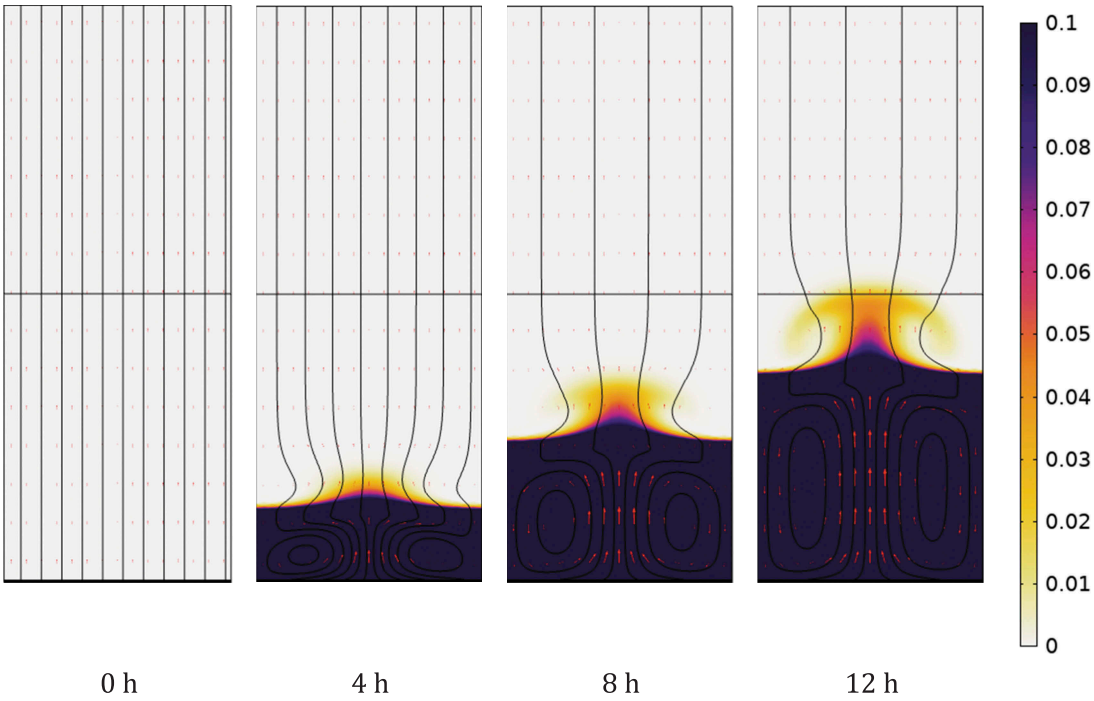

Fig. 9. Simulation of uranine propagating in a 1-mm-thick annulus with a sinusoidal light source. Note that the color bar is cut at $c = 0.1$ to clearly show the faster dye.

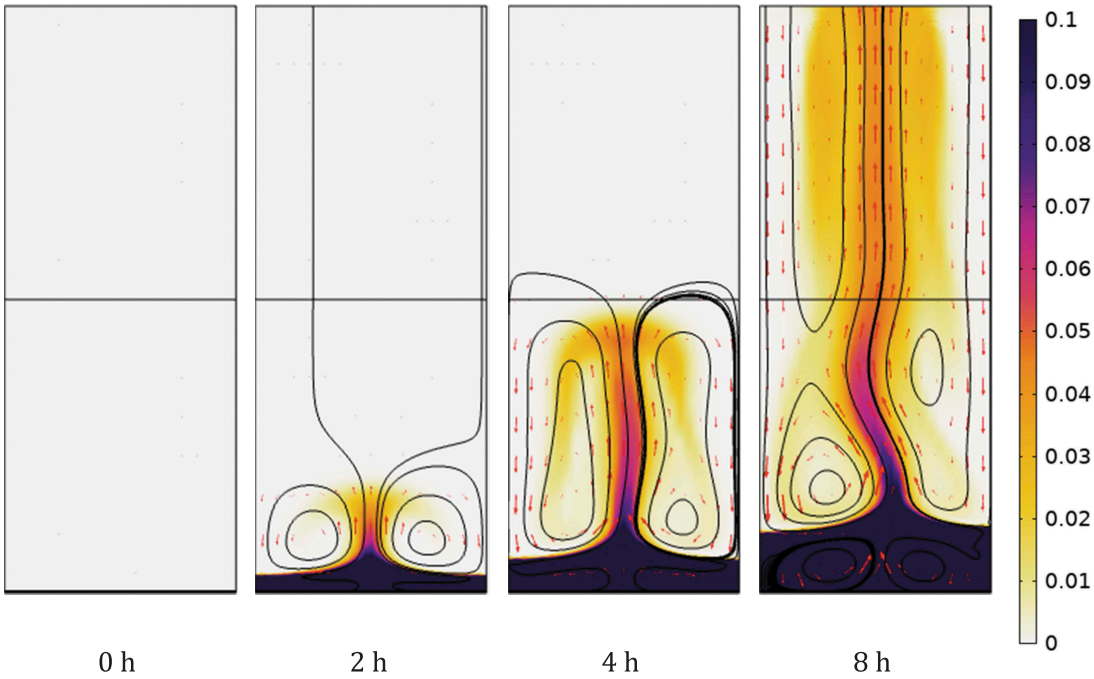

Fig. 10. Simulation of uranine propagating in a 2-mm-thick annulus with a sinusoidal light source. The color bar indicates the normalized concentration of uranine dye. Note that the color bar is cut at $c = 0.1$ to clearly show the faster dye.

acrylic glass sides replaced by one with granite (properties from COMSOL's Material Library) but without cooling by radiation or convection. The annuli were simulated as slots with thicknesses of 1 and 2 mm (80 cm high and 4.1π cm and 4.2π cm, respectively) with a sinusoidal light source to illustrate a light source facing one side of the column and a shadow side. The thickness of the acrylic glass was set to 0.5 cm. The heat capacity of the rock core on the inner side of the slot was also accounted for. The water was flowing upward with a flow rate of 50 μL/min, and the dye concentration was set to 1 g/L in the lowest section of the slot to mimic the injected pulse. The power flux was set to be on the order of 20 W/m^2, which is equivalent to approximately 2% of the power flux of direct sunlight.[32] The illumination was sinusoidal around the tube with 30 at the highest and 10 W/m^2 at the shadow sides. The simulated dye propagation for both annuli are shown in Figs. 9 and 10. Note that the color bar is cut at c = 0.1 g/L to clearly show the faster dye.

Disturbance of the flow field is clearly visible after a few hours. Note the rotation pattern establishing in the tracer domain in Fig. 9. After about 8 h a mushroom-shaped stream starts to protrude up into the water ahead of the stream. However, the model does not fully explain the fast streams as witnessed in these experiments. It is not clear if this is due to an underestimation of the light or an inability to account for other factors such as irregularities in room temperature, ventilation, irregular heat emanating from the laboratory environment, or other sources.

However, in Fig. 10, a much earlier onset of disturbance and a full stream that breaks out of the bulk flow are observed. The difference is due to the four times higher permeability. The simulated flow pattern is in accordance with the patterns observed in the laboratory experiment. The laboratory experiment showed patterns with curly veins of a higher uranine concentration surrounded by veils of a lower uranine concentration.

VII. DISCUSSION AND CONCLUSIONS

Figure 7 shows that for the moderate case where there is no solute exchange between the dye and bulk water, the uranine tracer in a 1-mm-aperture slot can be expected to generate buoyancy and instability when subject to illumination of 15 W/m^2. The simulated results for the tilted slot as shown in Fig. 8 indicate that circulation patterns develop due to the energy absorption of moderate lighting. While the simulation model cannot in detail reproduce the Rayleigh patterns and flow fields, it is shown that the available light is enough to induce rotation in the slot due to the light absorption. The heat-induced velocity of the fluid can be considerably larger than the low velocity in experiments aimed at the visualization of flow patterns in narrow slots and replicas of natural fractures.

The results in Fig. 9 do not fully manage to account for the flares experienced during the 1-mm experiment. However, in the 2-mm annulus, flaring streams similar to ones observed in laboratory experiments were obtained. It is not clear if this is due to an underestimation of the light or an inability to account for other factors such as irregularities in concentrations, room temperature, or other sources. The granite core, used in the COMSOL simulations described in Figs. 9 and 10, appears to be a large enough heat sink to stabilize the system to large extent.

We have by simple simulations investigated the arising artifacts experienced in some low-velocity tracer experiments, i.e., unexpected rising of dye through the bulk water. The results of the simulations of the two experiments described above show that light-induced heating of the tracer dye can explain the observed phenomenon.

Light-induced circulation can probably be avoided if a low light intensity is used when performing the experiments, preferably in complete darkness between observations. It is advisable to assess beforehand how the density of a tracer solution responds to visible white light as well as to blackbody radiation.

Another solution is to use tracers without light-induced effects, such as gases (e.g., Ref. 13), radioactive elements (e.g., Ref. 11), or saline tracers with electrical conductivity measurements (e.g., Ref. 33). However, when applying these tracers, one needs to compromise regarding the visualization of the flow patterns (gases), have access to radiochemistry laboratories, and use novel imaging techniques (radioactive elements) or accept higher detection limits (saline tracers).

Acknowledgments

The financial support from the Swedish Nuclear Fuel and Waste Management Company, SKB, is gratefully acknowledged. The transport experiments in the annular flow channel were performed as part of a study funded by Posiva Oy, whose financial support is also gratefully acknowledged.

ORCID

Helen Winberg-Wang http://orcid.org/0000-0002-2010-2894

References

1. J. W. ELDER, "Transient Convection in a Porous Medium," *J. Fluid Mech.*, **27**, *3*, 609 (1967); https://doi.org/10.1017/S0022112067000576.
2. C. I. VOSS and W. R. SOUZA, "Variable Density Flow and Solute Transport Simulation of Regional Aquifers Containing a Narrow Freshwater-Saltwater Transition Zone," *Water Resour. Res.*, **23**, *10*, 1851 (1987).
3. E. HOLZBECHER, *Modeling Density-Driven Flow in Porous Media*, 1st ed., Springer-Verlag, Heidelberg, Germany (1998).
4. F. MOUKALLED et al., "Buoyancy-Induced Flow and Heat Transfer in a Porous Annulus Between Concentric Horizontal Circular and Square Cylinders," *Numer. Heat Transfer A*, **69**, *9*, 1029 (2016); https://doi.org/10.1080/10407782.2015.1090847.
5. D. L. LÓPEZ and L. SMITH, "Fluid Flow in Fault Zones: Analysis of the Interplay of Convective Circulation and Topographically Driven Groundwater Flow," *Water Resour. Res.*, **31**, *6*, 1489 (1995); https://doi.org/10.1029/95WR00422.
6. "Long-Term Safety for the Final Repository for Spent Nuclear Fuel at Forsmark Main Report of the SR-Site Project," SKB TR-11-01, pp. L7–1L21, Svensk Kärnbränslehantering (SKB) (2011).
7. "Safety Case for the Disposal of Spent Nuclear Fuel at Olkiluoto—Performance Assessment 2012," Report 2012-04, Posiva Oy (2012).
8. S. JOYCE et al., "Groundwater Flow and Reactive Transport Modelling in ConnectFlow," SKB R-14-19, Svensk Kärnbränslehantering (SKB) (2015).
9. I. NERETNIEKS and H. WINBERG-WANG, "Density-Driven Mass Transfer in Repositories for Nuclear Waste," *Nucl. Technol.* (2018); https://doi.org/10.1080/00295450.2018.1537460.
10. H. WINBERG-WANG, "Diffusion in a Variable Aperture Slot: Impact on Radionuclide Release from a Repository for Spent Fuel," *Nucl. Technol.*, **204**, *2*, 184 (2018); https://doi.org/10.1080/00295450.2018.1469348.
11. M. VOUTILAINEN et al., "Laboratory Scale Advection-Matrix Diffusion Experiment in Olkiluoto Veined Gneiss Using H-3 and Cl-36 as Tracers," *MRS Adv.*, **2**, *12*, 655 (2017); https://doi.org/10.1557/adv.2016.675.
12. A. POTERI et al., "The First Matrix Diffusion Experiment in the Water Phase of the REPRO Project: WPDE 1," Working Report 2017-23, Posiva Oy (2018).
13. J. KUVA et al., "Gas Phase Measurements of Matrix Diffusion in Rock Samples from Olkiluoto Bedrock, Finland," *Transp. Porous Media*, **115**, 1 (2016); https://doi.org/10.1007/s11242-016-0748-1.
14. Adobe Photoshop® website; https://www.adobe.com/products/photoshop.html?promoid=PC1PQQ5T&mv=other (current as of Dec. 3, 2018).
15. D. H. SHARP, "An Overview of Rayleigh-Taylor Instability," *Physica D*, **12**, *1–3*, 3 (1984); https://doi.org/10.1016/0167-2789(84)90510-4.
16. ChemSpider website, ID15968; http://www.chemspider.com/Chemical-Structure.15968.html (current as of Aug. 27, 2018).
17. F. E. JONES and G. L. HARRIS, "ITS-90 Density of Water Formulation for Volumetric Standards Calibration," *J. Res. Nat. Inst. Stand. Technol.*, **97**, *3*, 335 (1992); https://doi.org/10.6028/jres.097.013.
18. R. SJÖBACK, J. NYGREN, and M. KUBISTA, "Absorption and Fluorescence Properties of Uranine," *Spectrochim. Acta Part A*, **51**, *6*, L7 (1995); https://doi.org/10.1016/0584-8539(95)01421-P.
19. T. W. MURPHY, "Maximum Spectral Luminous Efficacy of White Light," *J. Appl. Phys.*, **111**, 104909 (2012); https://doi.org/10.1063/1.4721897.
20. S. KOBAYASHI, S. MIKOSHIBA, and S. LIM, *LCD Backlights*, Wiley (2009).
21. W. Y. PARK et al., "Efficiency Improvement Opportunities in TVs: Implications for Market Transformation Programs," *Energy Policy*, **59**, 361 (2013); https://doi.org/10.1016/j.enpol.2013.03.048.
22. Z. LUO, Y. CHEN, and S.-T. WU, "Wide Color Gamut LCD with a Quantum Dot Backlight," *Opt. Express*, **21**, *22*, 26269 (2013); https://doi.org/10.1364/OE.21.026269.
23. R. B. BIRD, W. E. STEWART, and E. N. LIGHTFOOT, *Transport Phenomena*, 2nd ed., Wiley, New York (2002).
24. "Densities of Solids," Engineering ToolBox (2009); https://www.engineeringtoolbox.com/density-solids-d_1265.html (current as of Nov. 5, 2018).
25. "Air—Dynamic and Kinematic Viscosity," Engineering ToolBox (2003); https://www.engineeringtoolbox.com/air-absolute-kinematic-viscosity-d_601.html (current as of Nov. 5, 2018).
26. "Thermal Conductivity of Common Materials and Gases," Engineering ToolBox (2003); https://www.engineeringtoolbox.com/thermal-conductivity-d_429.html (current as of Nov. 5, 2018).

27. "Water—Thermal Conductivity," Engineering ToolBox (2018); https://www.engineeringtoolbox.com/water-liquid-gas-thermal-conductivity-temperature-pressure-d_2012.html (current as of Nov. 5, 2018).

28. "Specific Heat of Common Substances," Engineering ToolBox (2003); https://www.engineeringtoolbox.com/specific-heat-capacity-d_391.html (current as of Nov. 5, 2018).

29. "Air—Density, Specific Weight and Thermal Expansion Coefficient at Varying Temperature and Constant Pressures," Engineering ToolBox (2003); https://www.engineeringtoolbox.com/air-density-specific-weight-d_600.html (current as of Nov. 5, 2018).

30. R. FURUKAWA, J. LUIS, and B. WARE, "Self-Diffusion and Probe Diffusion in Dilute and Semidilute Aqueous Solutions of Dextran," *Macromolecules*, **24**, 599 (1991); https://doi.org/10.1021/ma00002a039.

31. COMSOL Multiphysics® 5.4 Modelling Software website; https://www.comsol.com/ (current as of Nov. 5, 2018).

32. "Energy from the Sun," American Chemistry Society; https://www.acs.org/content/acs/en/climatescience/energybalance/energyfromsun.html (current as of Nov. 26, 2018).

33. P. KEKÄLÄINEN et al., "Solutions to and Validation of Matrix-Diffusion Models," *Transp. Porous Media*, **87**, 125 (2012); https://doi.org/10.1007/s11242-010-9672-y.